Indian Journal of Engineering & Materials Sciences
Vol. 32, April 2025, pp. 211-224
DOI: 10.56042/ijems.v32i02.13424

Exploring the performance of three stage SPM-based regenerative wavelength conversion using HNLF

Parashuram[a], Chakresh Kumar[b]* & Ghanendra Kumar[c]

[a]Department of Electronics and Communication Engineering, Bharati Vidyapeeth's College of Engineering, New Delhi 110 063, India

[b]University School of Information, Communication & Technology, Guru Gobind Singh Indraprastha University, New Delhi 110 078, India

[c]University School of Automation and Robotics, Guru Gobind Singh Indraprastha University, New Delhi 110 078, India

Received: 28 August 2024; accepted: 07 January 2025

In this work, the effectiveness of three-stage highly nonlinear fiber (HNLF)-based self-phase modulation (SPM) regeneration wavelength conversion has been examined. Through the nonlinear Schrödinger equation (NLSE), nonlinear optical effects in fiber have been explored, which has been important to comprehend SPM-based conversion. In addition, mathematical exploration has been done on the principles of wavelength conversion, which have been mainly controlled by four-wave mixing (FWM), SPM, and cross-phase modulation (XPM). This work has offered the theoretical underpinnings of SPM-based wavelength conversion. We have investigated the features of HNLF, have delved into the architecture of the suggested three-stage conversion system, and have examined performance measures including optical power spectrum, RF spectrum quality factor (Q) and bit error rate (BER) in relation with bit rate (Gb/s). In the realm of regenerative wavelength conversion, this study has unveiled a spectrum of quality factor (Q) values across three consecutive stages, each associated with specific data rates. At a bit rate of 60 Gb/s, the quality factor at the first, second, and third stages for a 100 km length of HNLF has been achieved 19.36 dB, 19.39 dB, and 19.41dB. Additionally, realized quality factor at first, second, and third stages for a 50 km length of HNLF at a bit rate of 60 GB/s has been found as 24.96 dB, 25.26 dB, and 25.41 dB. It has been concluded from the findings that at each stage, bit error rate has reduced and quality factor has increased due to parallel combinations of OBPFs and 3R regeneration. The results have exquisitely highlighted the complex interaction between the number of stages used, HNLF length, and data rate for accomplishing optimal wavelength conversion of an optical signal from 1545 nm to 1555 nm.

Keywords: All optical wavelength conversion, Nonlinear optical effects, Nonlinear schrödinger equation, 3R regeneration

1 Introduction

Wavelength conversion is a crucial component of modern optical communication networks, enabling signal regeneration, wavelength routing, and network reconfiguration. There is a growing interest in creating effective and dependable wavelength conversion techniques due to the growing demand for flexible and high-capacity transmission networks. Using nonlinear optical effects for wavelength conversion applications in HNLFs is one promising strategy.Recent research has explored a range of topics in photonic integrated circuits and optical switching systems, covering areas such as deep neural network emulation, high-capacity optical switching, wavelength switching for load balancing, bi-directional wavelength conversion, photonic switching challenges, semiconductor optical amplifier advancements, and all-optical wavelength conversion systems[1-7].

Wavelength selective switches (WSS) play a crucial role in enabling dynamic and flexible wavelength routing in optical networks. In recent research, a noteworthy development in this domain was achieved with the experimental demonstration of a 1x4 WDM polarization-insensitive wavelength selective switch[8]. This device, based on bulk semiconductor optical amplifiers (SOAs) co-integrated with arrayed waveguide gratings (AWGs), exhibited promising characteristics such as net gain, broadband coverage, and error-free operation. Particularly significant was the minimal power penalty of 0.6 dB observed at data rates up to 25 Gbps non-return-to-zero on-off keying (NRZ-OOK), indicating its suitability for high-speed applications in optical networks. Lawan *et al.*[9] have conducted the study on the reduction of four-wave mixing efficiency in DWDM systems using optimal PMD. Their investigation focused on the impact of polarization mode dispersion (PMD) on the performance of

*Corresponding author (E-mail: chakreshk@ipu.ac.in)

nonlinear optical transmission systems within dense wavelength division multiplexing (DWDM) setups. Through systematic experimentation and simulation using Opti System software, they demonstrated the potential improvement in system performance with the presence of PMD. By optimizing PMD levels, they observed a significant reduction in fiber nonlinearities, leading to enhanced system efficiency. Their findings underscore the importance of considering PMD as a critical factor in system optimization efforts aimed at improving overall performance and efficiency in DWDM configurations. A recent study investigates how varying polarization states affect multicasting wavelength division multiplexing (WDM) networks and explores methods to mitigate resulting impairments[10]. The study reveals the adverse impact of polarization differences among neighboring channels, including SPM, XPM, PMD, and polarization-dependent loss (PDL), which degrade signal quality and constrain transmission distances and speeds in high-bit-rate optical links. By examining advanced strategies involving nonlinear optical phase conjugation (OPC) and dispersion compensation modules (DCMs) tailored for differently polarized channels, the study aims to effectively address these impairments. The proposed approach entails precise reversal of optical phase and amplitude distortions *via* OPC, coupled with meticulous dispersion compensation by DCMs, to counter nonlinearities and dispersion-induced impairments. Numerical simulations validate the effectiveness of this approach, particularly in enhancing the quality factor of DWDM networks amid random polarization fluctuations. An investigation has recently been conducted on an artificial neuron model based on nonlinear polarization rotation (NPR) within a semiconductor optical amplifier (SOA)[11]. This model utilizes NPR induced by bias current and optical injection to replicate a continuous sigmoidal neuron, with excitatory and inhibitory stimuli simulated accordingly. Fine-tuning of the initial state of polarization (SOP) enables precise control over the neuron's responsiveness, while insights into the effects of varying bias current and probe beam power on its output are also provided. The Manakov equation traditionally analyzes the nonlinear properties of PDM signal lights assuming orthogonally polarized states, this assumption may not hold in systems affected by PDL[12]. To bridge this gap, the study introduces a wave equation that accommodates the nonlinear interaction between non-orthogonally polarized PDM signals. Through derivation, the formula considers the impact of PDL-induced nonorthogonality. Calculations based on this formula demonstrate that the negligible errors incurred when employing the traditional Manakov equation with orthogonal PDM signals persist even when addressing nonorthogonal PDM signals affected by PDL. The combined effect of PMD and PDL on photon pairs traveling through different optical paths is demonstrated using density matrix and concurrence of the output state[13]. A fiber optic distributed acoustic sensor employing a double sagnac interferometer with two wavelengths separated by CWDM modules is investigated and introduces a mathematical model explaining the signal formation principle based on the analysis of signal shifts[14]. It investigates the sensor sensitivity dependency on disturbance coordinates and frequencies, facilitating sensor design optimization. Additionally, it presents an algorithm for data processing without filtering, suitable even under high system noise levels. Experimental validation of the sensor achieved an accuracy of 24 m over a 25.4 km single-mode fiber sensing fiber without requiring phase unwrapping. Recent investigations have explored various methods to address nonlinear impairments, including PMD, PDL, PDM, and FWM, across a range of applications such as wavelength conversion and tunability. These efforts aim to enhance the performance of DWDM optical links[15-18]. An approach is introduced to reduce the nonlinear effect of four-wave mixing (FWM) in fiber optic communication systems employing a dual port dual drive Mach-Zehnder modulator (DPDDMZ) and circular polarization to mitigate FWM[19]. This method is evaluated over a 100 km single-mode optical fiber with a 10 Gbps bit rate and 0.5 nm channel spacing. Compared to conventional systems using Mach-Zehnder modulators, their approach demonstrates superior FWM reduction. Specifically, the DPDDMZ-CP modulation technique significantly outperforms others, leveraging enhanced linearity and controlled signal chirp to achieve higher output signal power.A wavelength switchable erbium-doped fiber laser (EDFL) can be realized a tunable filter and a dual-pass Mach-Zehnder interferometer (MZI)[20]. The EDFL operates with erbium-doped fiber as the gain medium, achieving a laser working threshold of

92 mW. A dual-pass MZI, comprising three optical couplers and a variable fiber delay line, enhances laser stability. Tunable single- and dual-wavelength laser outputs are obtained, with stable performance demonstrated across various wavelength configurations. The study evaluates power fluctuations and achieves quadruple- and quintuple-wavelength laser outputs by adjusting intra-cavity loss. The wavelength conversion using four-wave mixing in a semiconductor optical amplifier (SOA) for quadrature amplitude modulation (QAM) signals is demonstrated[21]. It achieves successful conversion of 16 Gbaud 16-QAM signals across the C-band with low power penalty at the FEC threshold. Additionally, it achieves conversion of 5 Gbaud 64-QAM signals with a bit-error rate below the FEC threshold and the power penalty dependence on input OSNR with a single pump configuration is studied. Efficient modulation techniques and channel spacing play a significant role in improving the spectral efficiency of WDM long haul optical link[22]. Silicon waveguides have emerged as promising candidates for terahertz (THz) wave generation due to their advantageous properties compared to conventional silica-based optical fibers. A novel rib silicon waveguide based on the photonic crystal (PC) concept is introduced for the first time utilizing the scalar modulation instability (SMI) phenomenon[23]. Structural parameters such as the air-hole diameter of the PC and infiltration of optical fluids into the air holes are manipulated to control the linear and nonlinear characteristics of the waveguide, resulting in a tunable THz radiation source. Simulation results indicate that the maximum converted wavelength of 326.17 μm is achieved under specific conditions. Moreover, infiltration of optical fluids into PC air holes alters the dispersion properties of the waveguide, leading to additional converted wavelengths in the THz region. Importantly, the waveguide exhibits low loss, measuring less than 0.8 dB/cm. All-optical wavelength conversion technology, leveraging the four-wave mixing (FWM) effect, holds significant promise for modern high-speed optical signal processing systems. A novel dual-pump configuration, combining graphene with optical fibers, is proposed to mitigate the inherent polarization sensitivity of FWM[24]. Experimental results demonstrate that this configuration enhances FWM-based wavelength conversion efficiency by approximately 8 dB under parallel polarization states of dual pumps. Numerous recent studies have made significant contributions to the field, addressing diverse topics such as high-performance optical filtering, the impact of fiber-optic nonlinearities on long-haul and ultra-high-speed DWDM optical networks, compact waveguide-based wavelength conversion for complex modulation formats, polarization-insensitive all-optical wavelength conversion, optimization strategies for reducing maintenance issues in ultradense WDM systems, and rapid reconfigurable wavelength conversion techniques for advanced modulation formats[25-30]. An all-optical wavelength conversion (AOWC) scheme is demonstrated utilizing the four-wave mixing (FWM) effect in dual-polarization semiconductor optical amplifiers (SOAs) for processing 56 Gbps polarization division multiplexing 16-ary quadrature amplitude modulation (PDM-16QAM) signals[31]. Parallel dual-pump configurations are employed to enhance optical link capacity, maximizing spectrum utilization and bandwidth efficiency. The scheme achieves polarization insensitivity, allowing for the generation of wave signals at arbitrary polarization angles (θ). Analysis of wavelength conversion efficiency (CE) considers key parameters such as optical signal-to-noise ratio (OSNR), pump spacing, SOA injection current, and pump power. Optical circuit switches (OCS) present a viable solution to the challenges posed by the slowdown of Moore's law in scaling data center networks efficiently. By eliminating the need for costly and power-intensive transceivers and electrical switches, OCS based on tunable lasers and arrayed waveguide grating routers offer a promising approach. Leveraging a passive core enhances fault tolerance and reduces management overhead, resulting in a high-bandwidth, low-latency, and energy-efficient data center network. However, to efficiently support dynamic data center workloads, rapid wavelength switching at nanosecond (ns) timescales is imperative. The ultrafast OCS is investigated utilizing a microcomb and semiconductor optical amplifiers (SOAs). By employing a photonic integrated Si_3N_4 microcomb, sub-ns (<520 ps) switching is achieved alongside 25-Gbps non-return-to-zero (NRZ) and 50-Gbps four-level pulse amplitude modulation (PAM-4) burst mode data transmission[32]. Additionally, a photonic integrated circuit comprising an Indium phosphide-based SOA array and an arrayed waveguide grating demonstrates sub-ns switching (<900 ps) and 25-Gbps NRZ burst mode transmission, presenting a pathway towards a

more scalable and energy-efficient wavelength-switched network for data centers in the post Moore's Law era. Recent advances in integrated fabrication have enabled tiny chip-scale sagnac interferometers, which surpass classic devices in terms of size and scalability[33]. The advantages of the three-stage SPM-based regenerative conversion method with HNLF have been emphasized by recent research. Among these are: enhanced conversion efficiency, enhanced signal-to-noise ratio (SNR), and flexibility in bandwidth. HNLF's broad bandwidth coverage makes it possible to convert signals over a wide spectral range, which increases the conversion process' flexibility. However, recent studies have also identified a number of drawbacks with the three-stage SPM-based conversion method utilizing HNLF, such as: nonlinear effects managements, cost and complexity, and dispersion management. Improved conversion efficiency and low power penalty have been the main goals of recent efforts integrating HNLF into multi-stage conversion designs. Even so, a thorough examination of the three-stage SPM-based conversion process utilizing HNLF is still required, along with precise mathematical models and experimental validation, despite the promising results of current research.

In this work, we suggest a thorough examination of the three-stage SPM-based HNLF regenerative wavelength conversion process. In this study, we use HNLF, amplifiers and various combination of optical band pass filter to investigate the performance of a three-stage SPM based wavelength conversion system. This work seeks to explore the variation in signal quality by measuring the power spectrum, quality factor (Q) and bit error rate (BER) for different stages at varying data rates (Gb/s) integrating thorough mathematical models of nonlinear effects and system architecture through experimental validation. We aim to illustrate the viability and possible benefits of three-stage SPM-based conversion with HNLF in optical communication networks through this study.

2 Materials and Methods

2.1 Theoretical background

Nonlinear optical effects in optical fibers arise due to the interaction between the intense optical fields of propagating signals and the material properties of the fiber. These effects include Stimulated Raman Scattering (SRS), Stimulated Brillouin Scattering (SBS), Four-Wave Mixing (FWM), and SPM. Among these, SPM is particularly relevant to wavelength conversion as it induces a phase shift in the optical signal, leading to spectral broadening and consequently, wavelength conversion. The combination of the fiber's material qualities and the strong optical fields of propagating signals causes nonlinear optical effects in fiber. Complex equations constructed from the nonlinear Schrödinger equation (NLSE) and different nonlinear coefficients characterize these effects. One well-known nonlinear effect is SPM, which causes the optical signal to broaden in spectrum. The generalized NLSE, which takes into account both linear and nonlinear effects, can be used to characterize the behavior of optical signals propagating over HNLF. The NLSE considers the improved nonlinear coefficient (γ) in the context of HNLF. The NLSE governing the propagation of optical pulses in a fiber is given by equation (1),

$$i\frac{\partial A}{\partial z}+\frac{\beta_2}{2}\frac{\partial^2 A}{\partial t^2}+\gamma|A|^2A=0 \quad \ldots(1)$$

This equation describes the interplay between linear effects (dispersion) and nonlinear effects (such as self-phase modulation and four-wave mixing) in HNLF.$A(z,t)$represents the complex electric field envelope of the optical pulse, i is the imaginary unit, z is the propagation distance along the fiber, t is time, and β_2 is the group velocity dispersion coefficient. The FWM process is explicable mathematically as follows in equation (2),

$$i\frac{\partial A_3}{\partial z}+\gamma|A_1|^2A_3+\gamma|A_2|^2A_3+\gamma A_1A_2^*A_3=0 \quad \ldots(2)$$

where, the input optical waves are A_1 and A_2. The generated output wave is A 3. The propagation distance is represented by z, and the nonlinear coefficient is γ. In this equation, the term $|A_1|^2A_3$ represents the self-interaction of A_1 with itself, $|A_2|^2A_3$ represents the self-interaction of A_2 with itself, and $A_1A_2^*A_3$ represents the interaction between A_1 and A_2 resulting in the generation of A_3.Idler waves, or created signals, are referred to as A_3, whereas pump waves are generally defined as A_1 and A_2. Applications for the FWM process in optical fibers include optical amplification, signal regeneration, and wavelength conversion. It is a significant nonlinear phenomenon in optical fibers.

Reshaping of the optical signal can be achieved through nonlinear optical effects such as SPM or XPM in a nonlinear medium such as HNLF. The reshaping process is governed by the NLSE. Retiming

of the optical signal involves adjusting its timing to synchronize it with the system clock. This can be achieved through phase modulation techniques or by controlling the delay using delay lines. The retiming process can be represented by the phase modulation equation (3),

$$A(t) = A_0 e^{i\emptyset(t)} \quad \ldots(3)$$

where, $A(t)$ is the electric field envelope of the optical pulse at time t, A_0 is the initial amplitude of the optical pulse, and $\emptyset(t)$ is the phase modulation function. Alternatively, if delay lines are used for retiming, the delay can be represented by a time shift operator $T(\tau)$acting on the optical pulse as in equation (4),

$$A(t) = A_0 T(\tau) \quad \ldots(4)$$

where, $T(\tau) = t - \tau$, and is the τ time delay. To compensate the transmission losses, the optical signal is re-amplified by increasing its power. Optical amplifiers, such as erbium-doped fiber amplifiers (EDFAs), are commonly used to do this. Additionally, the reamplification process can be represented by the gain equation for the optical amplifier as,

$$P_{out} = GP_{in} \quad \ldots(5)$$

where, P_{out} is the output power of the optical signal after amplification, P_{in} is the input power of the optical signal, and G is the gain of the optical amplifier. In the presence of SPM, the optical signal experiences phase modulation proportional to its intensity. This leads to spectral broadening, effectively converting the signal to a new wavelength.

$$A_{out}(t) = A_{in}(t - \tau)e^{i\emptyset(t)} \quad \ldots(6)$$

where, $A_{in}(t)$ is the complex electric field envelope of the input signal, $A_{out}(t)$is the complex electric field envelope of the wavelength-converted signal, τ is the time delay, $\emptyset(t)$ is the phase modulation function induced by SPM. The phase change induced by SPM over HNLF in each stage can be represented as the integral of the intensity of the optical signal along the fiber length. Mathematically, the phase change $\Delta\emptyset^{(i)}(\lambda)$ at each wavelength λ in the i^{th} stage can be expressed as,

$$\Delta\emptyset^{(i)}(\lambda) = \int_0^L \gamma(\lambda, z)\left|{A_{in}}^{(i)}(z,t)\right|^2 dz \quad \ldots(7)$$

where, $\gamma(\lambda, z)$ is the wavelength dependent nonlinear coefficient of the HNLF, L is the length of HNLF in the i^{th} stage. The phase change experienced by the signal at each wavelength in each stage contributes to the overall spectral broadening and wavelength conversion. In this study, we investigate the performance of a three-stage wavelength conversion process utilizing HNLF, EDFA, optical bandpass filter (OBPF), and 3R regeneration. We analyze the impact of varying data rates (Gb/s) at each stage of wavelength conversion and assess the performance using quality factor (Q in dB) and bit error rates.

2.2 System architecture and operation

The proposed design, illustrated in Fig. 1(a), showcases a three-stage regenerative wavelength converter based on SPM. The experimental setup comprises a cascade of HNLF modules, optical amplifiers, filters, and signal analyzers. HNLFs are optical fibers specifically engineered to exhibit significantly higher nonlinear coefficients compared to conventional fibers. This enhanced nonlinearity allows for efficient nonlinear optical processes such as FWM and SPM, making HNLFs suitable for various applications including wavelength conversion, signal processing, and super continuum generation. The unique dispersion properties of HNLFs also contribute to their suitability for wavelength conversion tasks. The proposed wavelength conversion system consists of three stages, each utilizing SPM in HNLF to achieve wavelength conversion. In each stage, the input signal undergoes spectral broadening through SPM, followed by filtering to select the desired converted wavelength. The regenerated signal is then amplified and fed into the next stage for further conversion. This cascaded configuration enhances the conversion efficiency and enables regeneration of degraded signals. Each stage of wavelength conversion comprises a HNLF unit followed by EDFA. Initially, a 1545 nm optical signal is generated using a Pseudo Random Binary Sequence (PRBS) and an optical Gaussian pulse generator. This signal is then amplified by an EDFA 1 and filtered through OBPF 1 before entering a coupler. Simultaneously, a 1554 nm Continuous Wave (CW) assist beam is introduced into the coupler. The coupled signal then undergoes self-phase modulation within HNLF1, inducing a wavelength shift. Subsequently, the phase modulated signalis amplified by EDFA 2, before being split by a Fork 1x2_1. From one output port of this fork, the signal is directed towards the 3R regeneration cum receiver, while the other output feeds into the parallel combination of two optical band pass filters before being multiplexed through Fork 2X1_1, initiating the second stage of wavelength conversion. Following the

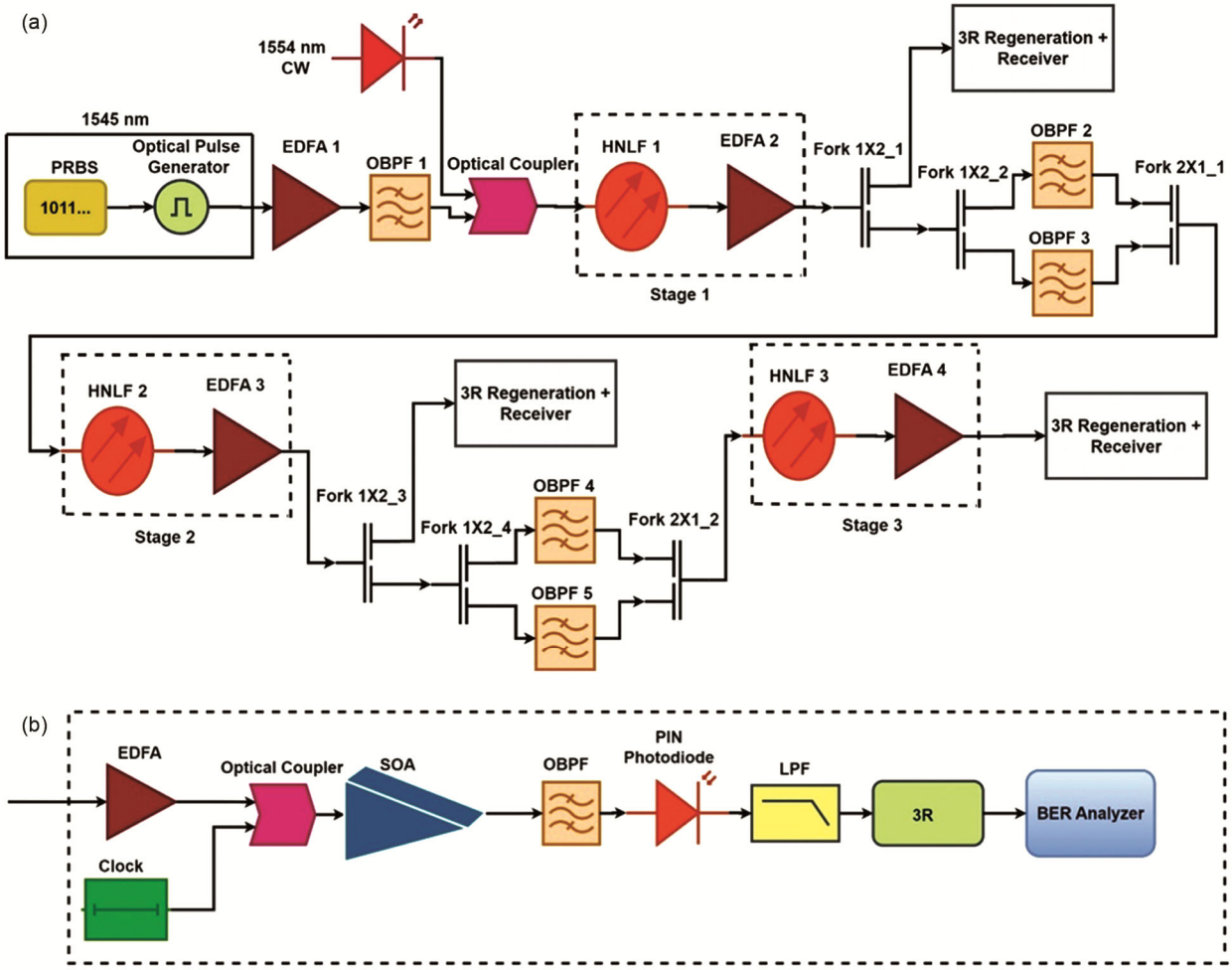

Fig. 1 — (a) Proposed setup of three stage SPM-based regenerative wavelength conversion using HNLF, and (b) 3R regeneration cum receiver.

second stage of wavelength conversion, a similar pattern is employed for third stage of wavelength conversion. At each stage, the performance of the wavelength converted signal is meticulously evaluated through the utilization of a 3R regeneration cum receiver, as depicted in Fig. 1(b). An EDFA amplifies a wavelength-converted signal through the process of simulated emission. The EDFA has a noise figure of 4 dB and a gain of 15 dB. An optical coupler is used to combine the outputs of the EDFA and a clock signal, which are then sent through a semiconductor optical amplifier (SOA). In order to synchronize with the incoming optical signal, the clock signal plays a crucial role in 3R regeneration. By coupling, the clock signal and the boosted optical signal line up exactly, allowing the regeneration mechanism to detect the timing of individual bits in the data stream. Since this synchronization makes it possible to precisely identify and restore the temporal structure of the optical pulses, it is essential for guaranteeing that the regenerated signal accurately replicates the original data. Through the establishment of this temporal reference, the clock signal helps regenerate the optical signal, effectively reshaping and retiming it to improve its quality and enable dependable data transmission. The SOA serves as a nonlinear element within the regeneration process. Its nonlinear response characteristics enable it to perform key signal processing functions, such as reshaping and retiming the optical pulses. By exploiting the nonlinear properties of the SOA, the regeneration process can mitigate distortions and optimize the signal quality. Moreover, the SOA contributes to the regeneration process by facilitating signal regeneration based on the clock signal. The incoming optical signal, along with the synchronized clock signal, is coupled into the SOA.

Through nonlinear interactions, the SOA effectively identifies the timing of individual bits within the data stream, aligning them with the clock signal. This temporal alignment ensures accurate retiming of the optical pulses, helping to restore the original temporal structure of the signal. After amplification and reshaping by the SOA, the optical signal passes through the Gaussian OBPF. The OBPF selectively allows signals within a specific wavelength range (the desired signal wavelength) to pass through while attenuating signals outside this range. This helps in removing noise and unwanted optical components from the signal. After that, a PIN photodiode detects the filtered signal and changes its optical form to electrical form. It converts the optical power into a corresponding electrical current based on the incident light intensity. This electrical current represents the regenerated signal in the electrical domain. After that, the electrical signal is subjected to additional processing, which includes going through a low-pass filter to get rid of high-frequency noise. The low pass filter attenuates these high-frequency components, allowing only the desired low-frequency signal (corresponding to the original data) to pass through. In order to ensure that the signal's quality is restored, it is finally subjected to 3R regeneration, which re-amplifies, reshapes, and retimes the signal pulses. A bit error rate tester is used to measure the accuracy of the regenerated signal's performance. In essence, the proposed design integrates self-phase modulation effectively across multiple stages, promising improved performance in optical communication systems through efficient wavelength conversion and signal regeneration. The performance of the three-stage conversion system is evaluated in terms of optical spectrum, RF spectrum, quality factor (Q) and bit error rate (BER). The system exhibits wide bandwidth coverage and robust operation over a range of input signal parameters, indicating its suitability for practical deployment in optical communication networks.

3 Results and Discussion

The proposed setup converts the wavelengths of an optical signal from 1545 nm to 1555 nm because of mutual interaction over nonlinear medium. The strong optical fields cause nonlinear effects in the medium when the optical signal travels through the HNLF. SPM reshapes and broadens the pulse's spectrum range by causing phase modulation of the optical pulse that is proportionate to its intensity. The simulation parameters of proposed setup are shown in Table 1.

The optical spectrum analyzer provides a visual representation of signal power distribution (dBm) across frequencies (nm). The power spectrum of a 1545 nm transmitted optical signal at the OBPF 1 is shown in Fig. 2(a). Optical Gaussian pulse generator

Table1 — Simulation parameters of the proposed setup.

Parameters	Value/Unit
Bit rate	up to 100 Gb/s
Transmitted signal wavelength	1545 nm
Assist beam wavelength	1554 nm
HNLF length	50 Km, 100 Km
Attenuation inside HNLF	2 dB/Km
Dispersion in HNLF	-0.1 ps/nm/km
Fract. Raman contribution	0.2
Orthogonal Raman factor	0.8
Noise figure of EDFA	4 dB
Gain of EDFA	15 dB
Gaussian OBPF bandwidth	0.6 nm (74.40 GHz)
Gaussian optical filter central wavelength	1554.8 nm
Low pass gaussian filter cut-off frequency	60 GHz
Responsivity of photodetector PIN	0.9 A/W
Dark current of photodetector PIN	9.8 nA

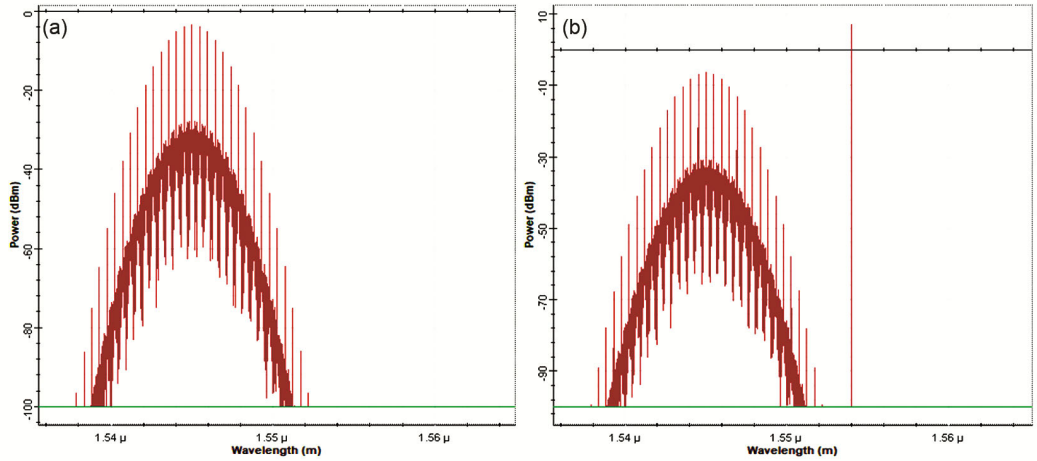

Fig. 2 — Optical spectrum at (a) OBPF 1 (transmitted optical signal), and (b) Optical coupler (Probe signal + Pump signal).

is used to transmit the optical signal followed by EDFA amplifier with 4 dB noise margin. Peak power is -28 dBm at 1545 nm in a span of 1538 nm to 1552 nm. Figure 2(b) depicts the optical spectra at the optical coupler after combining the 1545 nm Gaussian probe signal and a CW assist beam at 1554 nm. Launched power of CW assist beam is 10 dBm while power received after coupling is 7 dBm. At pre-conversion state, the OBPF's bandwidth and center wavelength are taken to be 0.025 nm and 1545 nm, respectively. Figure 3(a & b) depict the optical spectra after first stage wavelength conversion, observed at the EDFA 2 after passing through HNLF 1 and the Fork 1X2_1 succeeded by 3R regeneration cum receiver, respectively. At 1545 nm, the power level reads -26 dBm, while at 1555 nm, it drops to -46 dBm, as observed at EDFA 2. Power spectrum of Fig. 3(a) includes the assist beam at 1554 nm with 5 dBm power. Following the first stage conversion, the optical spectrum experiences a notable displacement towards longer wavelengths, with the central peak transitioning from 1545 nm to 1555 nm. The original signal, which peaked at 1545 nm, is nearly exhausted as its power level falls below -94 dBm, as shown in Fig. 3(b). The same signal is then shifted to 1555 nm, where its peak power is -32 dBm. Importantly, the noise level remains below -100 dBm post first-stage wavelength conversion, indicating a commendable signal-to-noise ratio. The peak's amplitude typically correlates with the signal power at the converted wavelength.

Figure 4 illustrates the optical power spectrum following thesecond stage of wavelength conversion, while Fig. 5 depicts the spectrum after the third stage

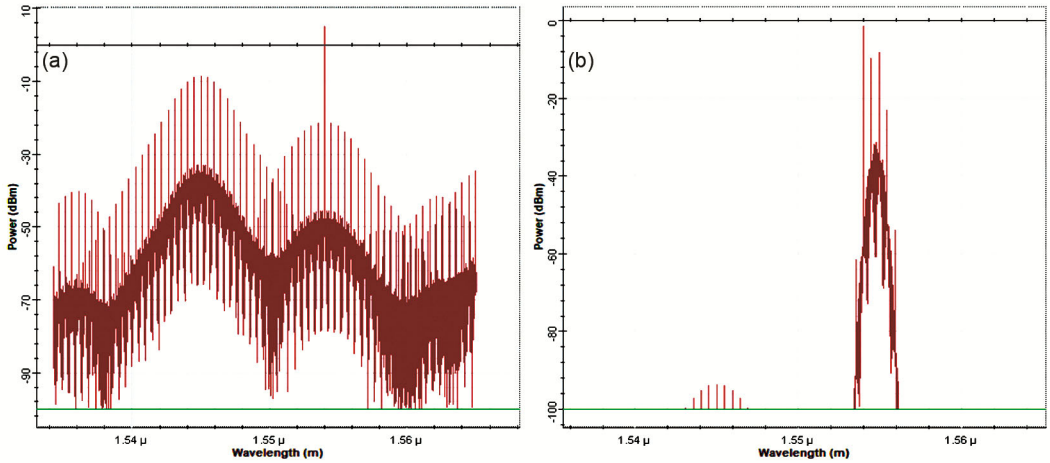

Fig. 3 — Optical spectrum after first stage wavelength conversion at (a) EDFA 2, and (b) 3R regeneration cum receiver (via Fork 1X2_1).

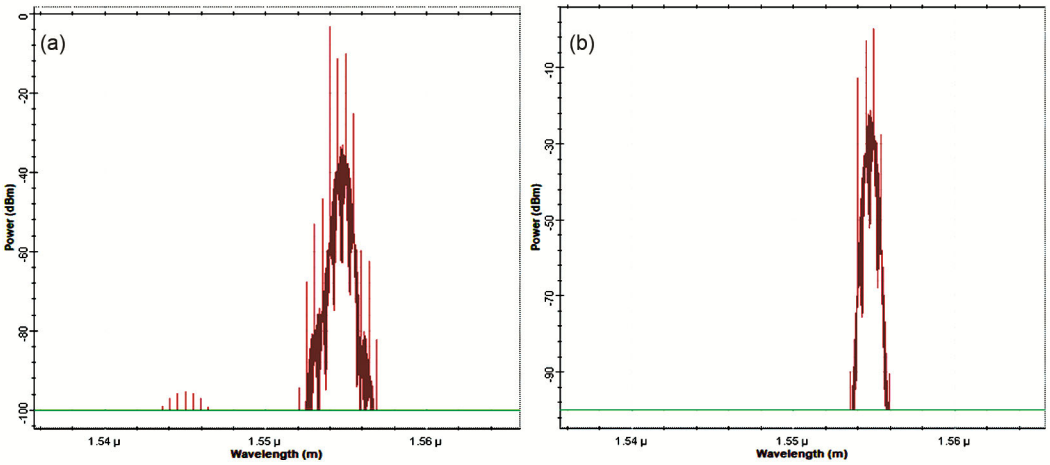

Fig. 4 — Optical spectrum after second stage wavelength conversion at (a) EDFA 3 and (b) 3R regeneration cum receiver (via Fork 1X2_4).

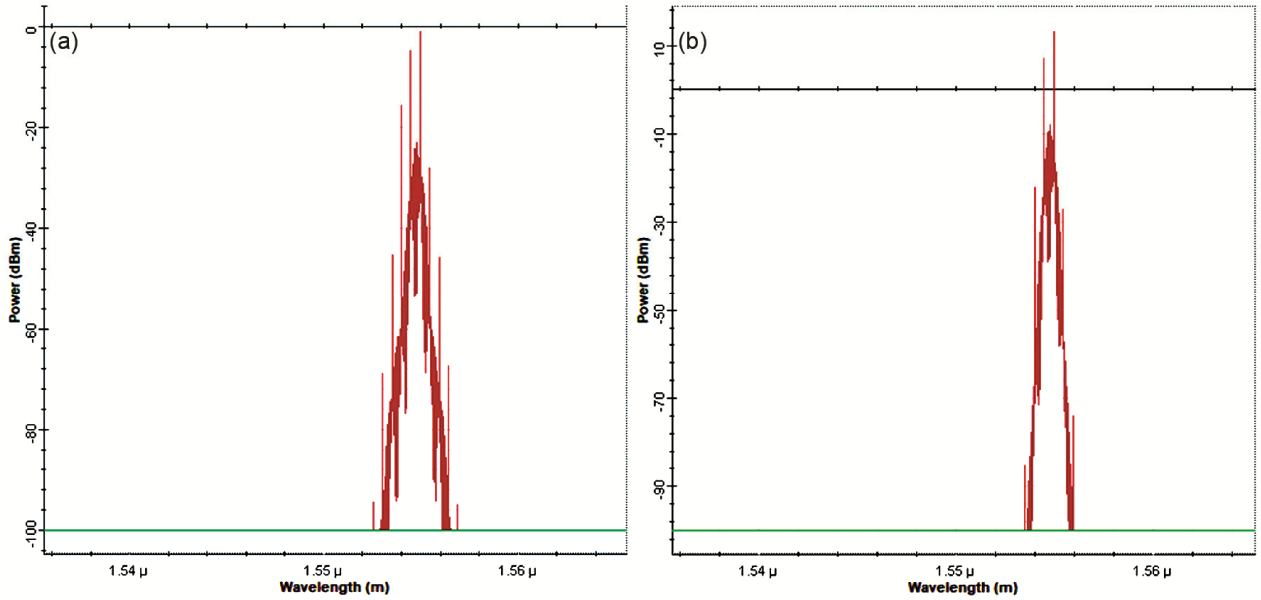

Fig. 5 — Optical spectrum after third stage wavelength conversion at (a) EDFA 4 and (b) 3R regeneration cum receiver.

of the conversion. After passing through HNLF 2 following second stage wavelength conversion, the optical spectrum at EDFA 3 is displayed in Fig. 4(a). The original transmitted 1545 nm signal is nearly completely depleted and has shifted to 1555 nm at this point, as evidenced by the power level of the signal centered at 1545 nm being below -96 dBm and the power level at 1555 nm being at -33 dBm. With several nearby sidebands and a complete shift in signal to a range of 1553–1556 nm, as shown in Fig. 4(b), the power level at 1555 nm is -21 dBm following the 3R regeneration. Furthermore, after passing through HNLF 3 following third stage wavelength conversion, the optical spectrum at EDFA 4 is displayed in Fig. 5(a). The original transmitted 1545 nm signal is nearly completely depleted and has shifted to 1555 nm at this point, as evidenced by the power level of the signal centered at 1545 nm being below the noise level (<-100 dBm) and the power level at 1555 nm being at -22 dBm. With several nearby sidebands and a complete shift in signal to a range of 1554–1556 nm, as shown in Fig. 5(b), the power level at 1555 nm is -8 dBm following the 3R regeneration. OBPF deplete the unwanted signal at this stage and received signal is centered around 1555 nm. For simulation, the OBPF's bandwidth and center wavelength are taken to be 0.6 nm and 1555 nm, respectively, post conversion at each stage. From the different spectrums, it can be inferred that the signal power level increases with each conversion

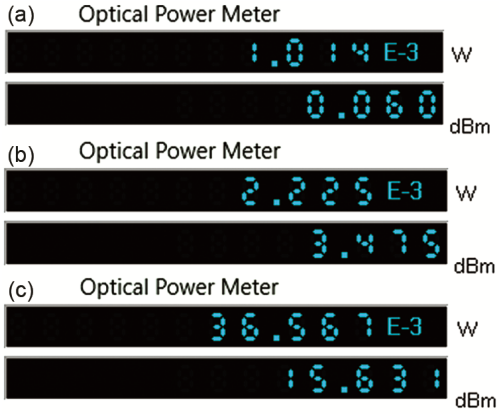

Fig. 6 — Received optical power at 80 Gb/s after (a) First stage conversion, (b) Second stage conversion, and (c) Third stage conversion.

stage and that sidebands decrease as a result of EDFAs, HNLFs, parallel combination of optical band pass filters and 3R regeneration cum receivers.

The received optical power at 80 Gb/s post-wavelength conversion, following amplification and filtering, is displayed in Fig. 6. The power measured using optical power meter at the first, second, and third stages is 0.06 dBm, 3.475 dBm, and 15.631 dBm, in that order. It has been noted that 3R regeneration causes power to increase after each stage.

The RF spectrum of the retrieved electrical signal at the receiving end is displayed in Fig. 7. Following wavelength conversion, the signal passes through a 3R regeneration cum receiver at each stage. The

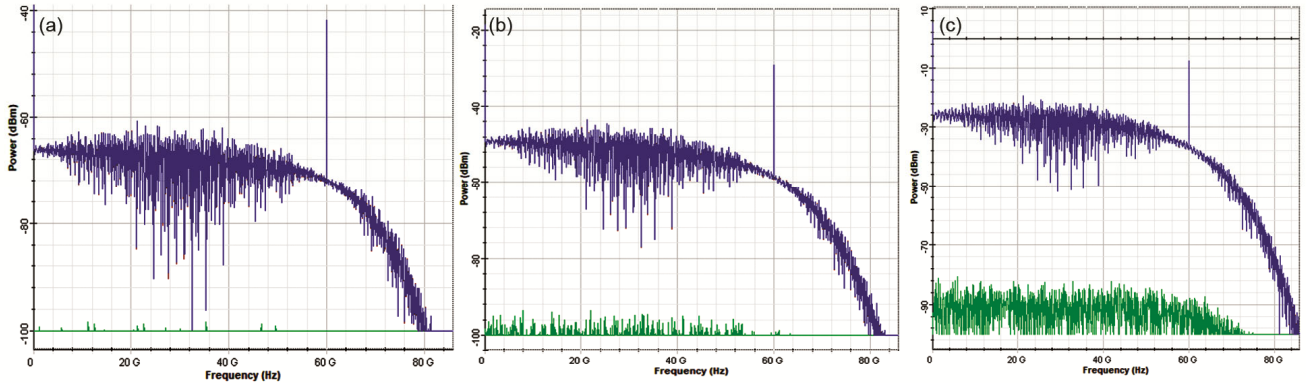

Fig. 7 — Received electrical power as a function of the frequency, at 60 Gb/s. RF spectrum at the output after (a) First stage, (b) Second stage and (c) Third stage.

photodetector PIN converts the optical signal back to an electrical signal with a responsivity of 0.9 A/W and a dark current of 9.8 nA. After conversion, the electrical signal is sent through a low-pass Gaussian filter with a 60 GHz cutoff frequency. The electrical power distribution across the frequency range of 0 to 80 GHz is measured using the RF spectrum analyzer. The electrical signal power for first stage conversion throughout a 60 GHz frequency range is displayed in Fig. 7(a). The low pass Gaussian filter keeps the electrical power level above -72 dBm until 60 GHz, at which point it starts to drop. The optical to electrical conversion process losses result in a low power level of the electrical signal (>-72 dBm) at 60 Gb/s. However, the noise power level is below -100 dBm, indicating a better signal to noise ratio (SNR). Moreover, The RF spectrum depicted in Fig. 7(b) depicts the power level of an electrical signal in relation with frequency range for the second stage wavelength conversion. It indicates that the power of the electrical signal exceeds -60 dBm, whereas the noise power is -94 dBm. It indicates that at 60 Gb/s, noise power increases in tandem with signal power due to 3R regeneration, while signal-to-noise ratio increases after the second step of conversion. Additionally, Fig. 7(c) depicts the RF spectrum plot following the third stage of 3R regeneration and wavelength conversion at 60 Gb/s. It has been reported that electrical signal power exceeds -38 dBm over a 60 GHz bandwidth, whereas noise power is less than -82 dBm. This suggests that the power of the electrical signal increases at a faster rate at this stage and simultaneously noise power increases effectively increasing SNR. As a result, signal quality is determined by both data rate and the number of stages of wavelength conversion, necessitating a

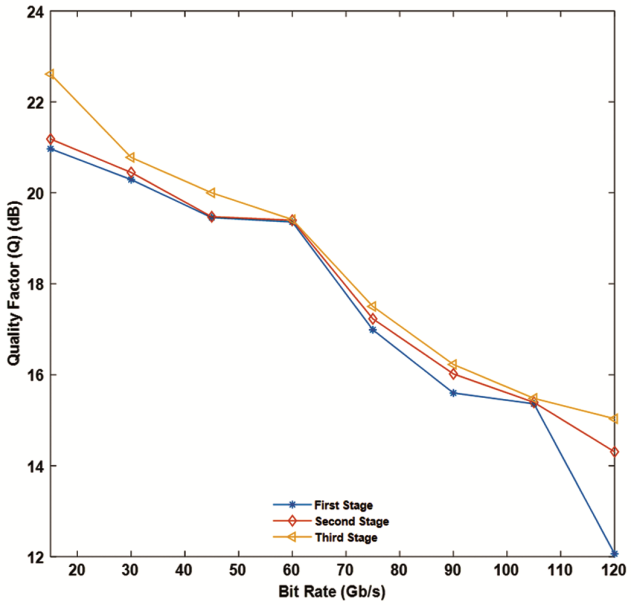

Fig. 8 — Quality factor (Q, dB) in relation with bit rate (Gb/s), for L=100 Km.

trade-off in order to achieve the optimal outcome for an optical DWDM link.

The quality factor (Q, dB) as a function of bit rate (Gb/s) is displayed in Fig. 8 for 100 Km length of HNLF at each stage. Additionally, the bit error rate variation in relation to the changing bit rate (Gb/s) is displayed in Fig. 9 for 100 Km length of HNLF at each stage. After every stage, bit error rate is seen to drop concurrently with an increase in quality factor. The results validate this strong correlation. as shown by Fig. 8 and Fig. 9.Every stage has HNLF followed by EDFA to add the nonlinearity which causes phase shift that creates the required wavelength shift. The impact of nonlinear impairments is also mitigated at each stage by adding the parallel combination of

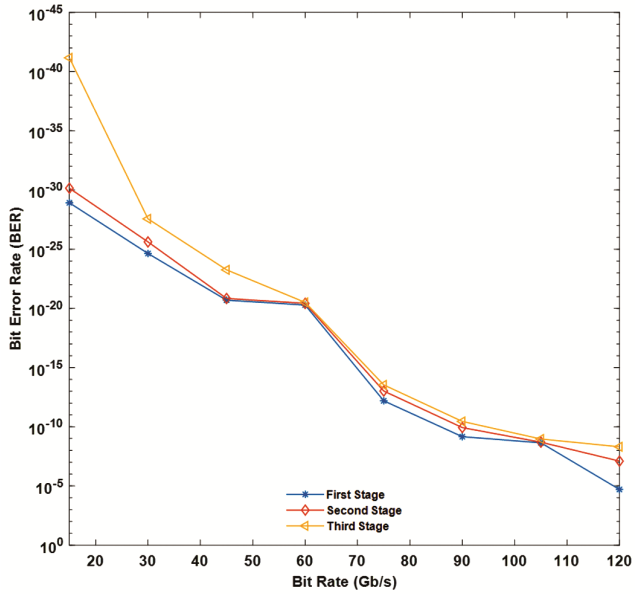

Fig. 9 — Bit error rate (BER) in relation with bit rate (Gb/s), for L=100 Km.

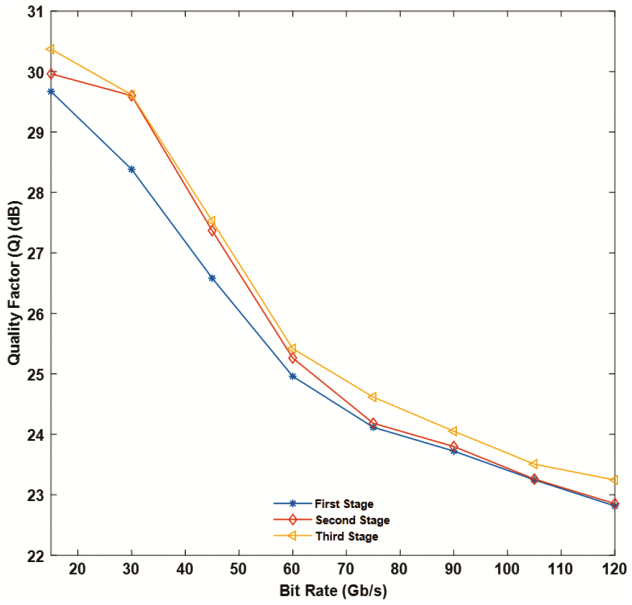

Fig. 10 — Quality factor (Q, dB) in relation with bit rate (Gb/s), for L=50 Km.

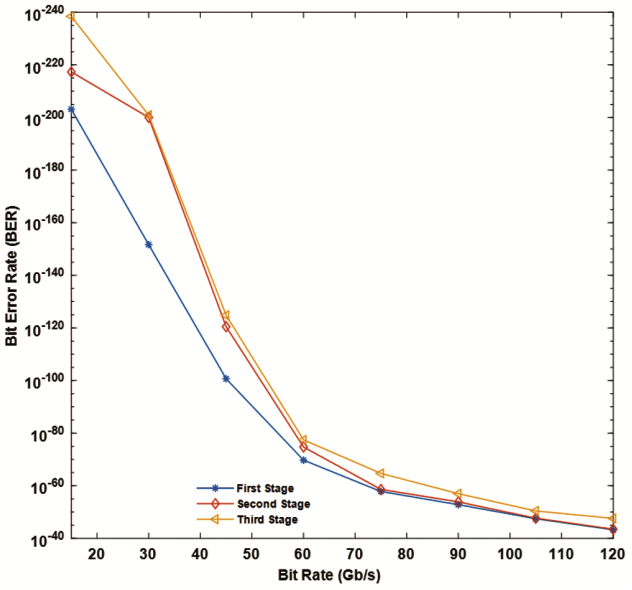

Fig. 11 — Bit error rate (BER) in relation with bit rate (Gb/s), for L=50 Km.

OBPFs and 3R regeneration, which raises the quality factor while concurrently lowering the BER.The 3R regeneration procedure helps to reduce noise power and increase received signal power at each stage. Wavelength conversion module consists HNLF followed by EDFA. Wavelength converted signal passes through OBPFs follower by 3R regeneration to obtain a quality signal at desired wavelength.

The quality factor for a 100 km fiber length at 15 Gb/s is 20.96 dB, 21.18 dB, and 22.61 dB for the first, second, and third stages, respectively. Furthermore, the quality factor at 120 Gb/s is 12.06 dB, 14.30 dB, and 15.03 dB for the first, second, and third stages, respectively. The bit error rate for a 100 km fiber length at 15 Gb/s is 1.21×10^{-29}, 7.07×10^{-31}, and 6.82×10^{-42} for the first, second, and third stages, respectively. Furthermore, the bit error rate at 120 Gb/s is 1.96×10^{-5}, 7.93×10^{-8}, and 4.89×10^{-9} for the first, second, and third stages, respectively.For an HNLF length of 50 Km at each stage, the quality factor (Q, dB) and bit error rate curves as a function of bit rate (Gb/s) are displayed in Fig. 10 and Fig. 11, respectively. Shortening the highly nonlinear fiber significantly boosts the system's performance. Signal quality is expressed in terms of Q and BER for bit rates ranging from 15 Gb/s to 120 Gb/s. At each stage, the utilization of a 50 km HNLF consistently yields a higher quality factor and a correspondingly lower bit error rate compared to its 100 km counterpart. Additionally, as the signal progresses through subsequent stages, there is a noticeable increase in the quality factor accompanied by a corresponding decrease in the bit error rate. For instance, at a bit rate of 60 Gb/s, the quality factors and corresponding bit error rates for the first, second, and third stages are observed to be 24.96 (BER= 1.9×10^{-70}), 25.26 (BER=1.92×10^{-75}), and 25.41 (BER= 3.65×10^{-78}), respectively. Compared to a longer HNLF length (100 km), a

shorter HNLF length (50 km) yields significantly higher Q-factors and lower BERs. This suggests that shortening the nonlinear fiber length enhances system performance by lowering nonlinear effects and signal distortions at all tested bit rates. The enhancement in Q-factor and decrease in BER across all stages demonstrate how the parallel combining of Optical Bandpass Filters (OBPF) after each stage of wavelength conversion helps to preserve signal integrity and reduce noise. After each stage of wavelength conversion, 3R (Re-amplification, Retiming, and Reshaping) regeneration is included to help reduce signal degradation and maintain signal quality over several stages, allowing high-speed data to be transmitted with minimal errors. This observation emphasizes the importance of striking an optimal balance between the number of stages, data throughput (bit rate), HNLF length and the integration of 3R regeneration to effectively enhance overall system performance.

At a data rate of 60 Gb/s, the eye diagrams with eye patterns are shown in Fig. 12. The eye diagram is a graphical depiction of the quality of a digital signal, with eye height expressed in micrometers against bit period. Following wavelength conversion, the eye diagrams at the first, second, and third stages are displayed in Fig. 12(a), 12(b), and 12(c). The resulting eye diagrams showed diverse heights, which were indicative of various signal characteristics. At a transmission rate of 60 Gb/s, the measured heights at the first, second, and third stages correspond to quality factors are 1.46 mm (Q=24.96 dB), 10.32 mm (Q=25.26 dB), and 136.67 mm (Q=25.41 dB), respectively. The signal-to-noise ratio and distortion levels in the suggested optical link are reflected in quality factors. The eye height is quite high at 60 Gb/s after third-stage wavelength conversion, but noise gradually increases with progress of number of stages because of nonlinear media at each stage. This is caused by jitters because EDFA amplifies the signal power at each stage while simultaneously raising the noise level due to several wavelength conversion stages. To raise the Q value at every stage, EDFA, a set of optical band pass filters connected in parallel, and 3R regeneration must be optimized.As the wavelength conversion progresses, the eye height rises, indicating a gradual improvement in signal quality in later stages. This increase highlights a methodical improvement in signal processing and integrity preservation throughout the conversion process and can be linked to the evolution of 3R regeneration techniques applied at each stage.

By causing phase and amplitude variations in the signal, XPM, which happens when numerous optical signals interact within the medium, can also aid in signal reshaping. SOA efficiently reshapes the optical pulse, compensating for distortion and preserving signal integrity by adjusting the parameters of the nonlinear medium and the input signal. Retiming involves adjusting the timing of the optical signal to synchronize it with the receiver's clock. The Optical Regenerator retimes the optical pulses by removing timing jitter and adjusting the phase of the signal. This ensures proper synchronization between transmitted and received signals, improving signal recovery and reducing timing errors. In order to offset transmission losses, reamplification entails increasing the power of the optical signal. Optical amplifiers, such as EDFAs, are used by the Optical Regenerator to reamplify optical pulses. This method makes sure there is enough signal strength for additional transmission or processing by returning the signal to its initial power level.

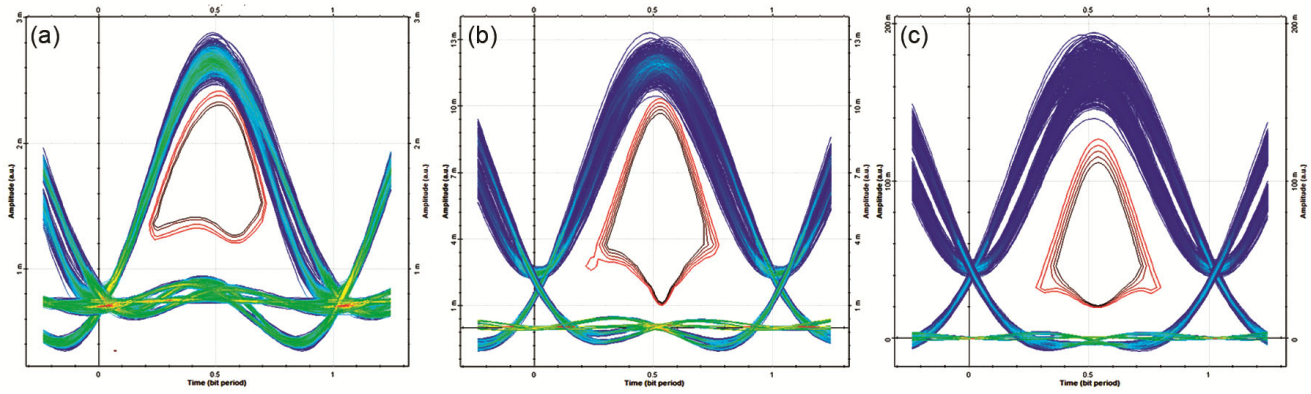

Fig. 12 — Eye diagrams of converted signal at 60 Gb/s for (a) First stage, (b) Second stage and (c) Third stage.

The efficacy of the three-stage SPM-based wavelength conversion system with HNLF is validated by experimental data. With minimal signal degradation, the system maintains a high-quality factor and low bit error rates even at increased data rates. The system's resilience and adaptability are demonstrated by the examination of the bit error rate and Q value in dB following each wavelength conversion step. The proposed conversion technique for optical communication networks is discussed with an emphasis on its possible applications and practical issues.

4 Conclusion

This paper presents a comprehensive investigation into the performance of three-stage SPM-based regenerative wavelength conversion using HNLF. The results show how good it is to use several wavelength conversion stages in an optical communication network that includes amplification, parallel combination of OBPFs, and 3R regeneration unit at each stage. It is feasible to provide reliable high-speed data transmission with improved signal quality and low error rates by combining these elements. Additionally, cutting the highly nonlinear fiber's length significantly improves the system's performance. Thus, the total performance of the optical communication link can be greatly improved by optimizing the design parameters, such as HNLF length and bit rate. The results indicate that for a 100-kilometer long HNLF, at a bit rate of 60 Gb/s, the first stage exhibited a minimum quality factor of 19.36 and a bit error rate of 5.2×10^{-21}; the second stage showed a slightly higher quality factor of 19.39 and a bit error rate of 3.75×10^{-21}); most notably, the third stage had a higher quality factor of 19.41 and a bit error rate of 3.12×10^{-21}). Furthermore, for a 50-kilometer long HNLF, for the first, second, and third stages, respectively, a notable increase in quality factor attainment is noted, with values of 24.96 (with a bit error rate of 1.9×10^{-70}), 25.26 (with a bit error rate of 1.92×10^{-75}), and 25.41 (with a bit error rate of 3.65×10^{-78})at a bit rate of 60 Gb/s. These results suggest that nonlinearity, which is added by HNLF and then EDFA at each stage to achieve the necessary shift in wavelength, is normalized by using a parallel combination of OBPF and 3R regeneration at each stage. These findings underscore the intricate interplay between the number of stages employed, fiber length and the associated data rate, vital for achieving optimal wavelength conversion of an optical signal from 1545 nm to 1555 nm.

The proposed conversion scheme holds great potential for enhancing the flexibility and efficiency of optical communication networks, paving the way for future advancements in wavelength conversion technologies. Although it performs well, there are still a few issues that need to be resolved before SPM-based wavelength conversion with HNLF can be widely used. These include integrating the conversion system with the current network infrastructure, minimizing nonlinear effects, and optimizing system parameters for particular network topologies. Prospective research avenues could center around the advancement of sophisticated nonlinear mitigation methods, investigation of innovative fiber materials, and improvement of system scalability and compatibility with developing optical network technologies.

References

1 Shi B, Calabretta N & Stabile R, *Neuromorph Comput En*, 2(3) (2022) 034010.
2 Mendinueta J M D, Shinada S, Hirota Y, Furukawa H & Wada N, *IEEE J Sel Top Quant*, 26 (4) (2020).
3 Kaur H & Kaler R, *Opt Eng*, 59(11) (2020) 117109.
4 Amiri I S, Rashed A N Z, Mohammed A E A & Aboelazm M B, *J Opt Commun*, 45(s1) (2019) s41.
5 Yoo S J B, *J Lightw Technol*, 40(8) (2022) 2214.
6 Sobhanan A, Anthur A, O'Duill S,Pelusi M, Namiki S, Barry L, Venkitesh D & Agrawal G P, *Adv Opt Photonics*, 14(3) (2022) 571.
7 Kong X & Zhao Y, *Opt Fiber Technol*, 63 (2021) 102480.
8 Zali A R, Stabile R & Calabretta N, *Optical Fiber Communication Conference, San Diego: Optica Publishing Group*, ISBN 978-1-957171-18-0 (2023).
9 Lawan S H & Mohammad A B, *Opt Quant Electron*, 50(2) (2018) 91.
10 Parashuram & Kumar C, *J Opt*, 53(5) (2024) 4772.
11 Li Q , Wang Z, Wang H, Cui C & Wu C, *Opt Commun*, 435 (2019) 405.
12 Inoue K & Igarashi K*, Optics Continuum*, 2(10) (2023) 2225.
13 Liu Y*, Opt Quantum Electron*, 55 (8) (2023) 720.
14 Zhirnov A A, Choban T V, Stepanov K V, Koshelev K I, Chernutsky A O, Pnev A B & Karasik V E, *Sensors*, 22(7) (2022) 2772.
15 Kaler R & Kaur G, *Optoelectron Adv Mat*, 15 (2021) 49.
16 Parashuram & Kumar C, *J Opt*, 53(2) (2023) 1471.
17 Huo J, Wang J, Wang Y, Shang C, Huangfu W, Liu L, Wang Z, Long K & Wu C, *Appl Opt*, 61(13) (2022) 3754.
18 Sharma N, Singh H & Singh P, *Proceedings of the 5th International Conference on Communication and Electronics Systems (ICCES)*, (2020) 343.
19 Sabat N K, Rao B S & Patnaik, *IEEE-ICACCI*, (2017) 1946.
20 Wei W, Li Q,Wang Y & Duan J, *Phys Scripta*, 97(8) (2022).
21 Filion B, Ng W C, Nguyen A T, Rusch L A & LaRochelle S, *Opt Express*, 21(17) (2013) 19825.

22 Parashuram & Kumar C, *Indian J Pure Ap Phy*, 60(8) (2022) 23.
23 Yang Y, Duan M, Lin J, Wang Z, Wang K, Ji J & Song Y, *Opt Express*, 30(6) (2022) 10168.
24 Hosseinabadi S, *J Nonlinear Opt Phys Mater*, 28(01) (2019) 1950002.
25 Arianfard H, Wu J, Juodkazis S & Moss D J, *Proc SPIE 11691*, Silicon Photonics XVI, 11691 (2021) 1169107.
26 Ali F, Khan Y, Qureshi S S, Ahmad S & Waqas M, *J Opt Commun*, 43(1) (2022) 39.
27 Ettabib M A, Lacava C, Liu Z, Bogris A, Kapsalis A, Brun M, Labeye P, Nicoletti S, Syvridis D, Richardson D J & Petropoulos P, *Opt Express*, 25 (2017) 3252.
28 Anthur A P, Zhou R, O'Duill S, Walsh A J, Martin E, Venkitesh D & Barry L P, *Opt Express*, 24(11) (2016).
29 Chauhan A, Vaish A & Verma A , *J Opt Commun*, 41(4) (2020) 421.
30 Lin Y, Anthur A P, O'Duill S, Liu F, Yu Y & Barry L P, *Appl Sci*, 7 (2017) 1033.
31 Zhao Y, Yan Z, Fu P, Cai Y & Yuan Y , *OSA Continuum*, 4(4) (2021) 1125.
32 Raja A S, Lange S, Karpov M, Shi K, Fu X, Behrendt R, Cletheroe D, Lukashchuk A, Haller I, Karinou F, Thomsen B, Jozwik K, Liu J, Costa P, Kippenberg T J & Ballani H, *Nat Commun*, 12 (2021) 5867.
33 Arianfard H, Juodkazis S, Moss D & Wu J, *Appl Phys Rev*, 10(1) (2023) 011309.